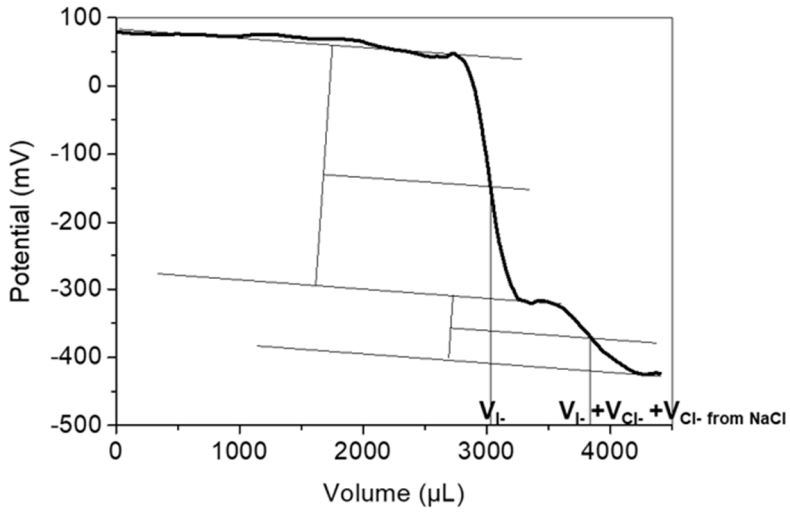


(**a**)

Sample	Incorporated chloride content (%)	V_{I^-}/V_{Cl^-} (µL)	Real chloride content (%)
PK 2-1	50	3010 / 357	10
PK 3-1	40	1863 / 794	30
PK 4-1	33	2362 / 643	21
PK 5-1	28	2106 / 439	17

(**b**)

Figure S1. (**a**) Typical potentiometric titration curve (example for PK 2-1); (**b**) Table for the calculation of equivalent volumes and chloride contents.

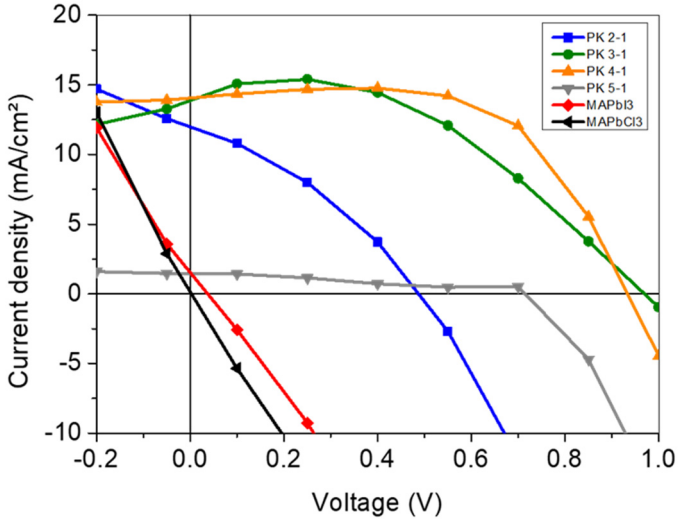


Figure S2. Representative JV curves of AZO-based PV cells realized using different perovskite precursors compositions.

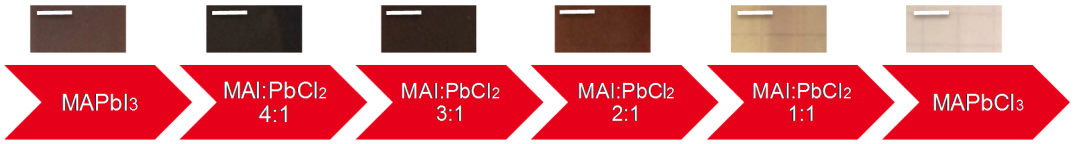
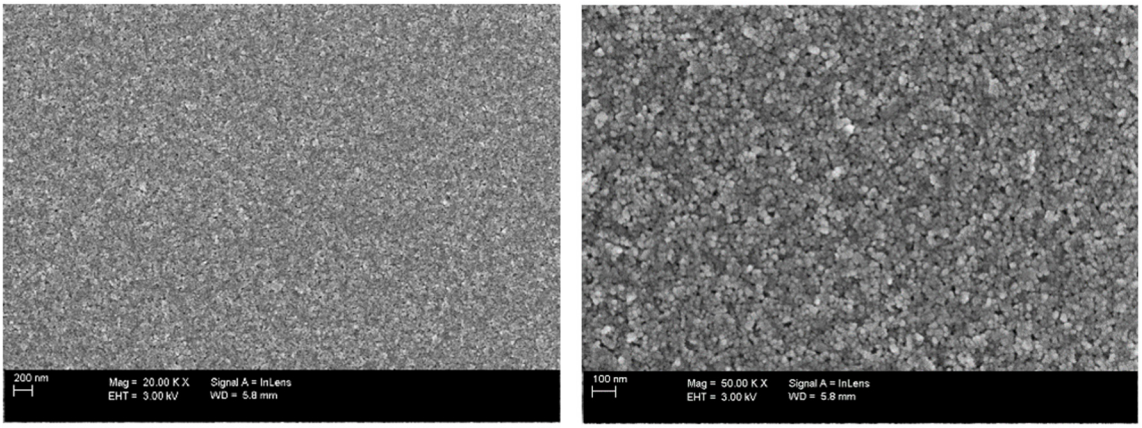
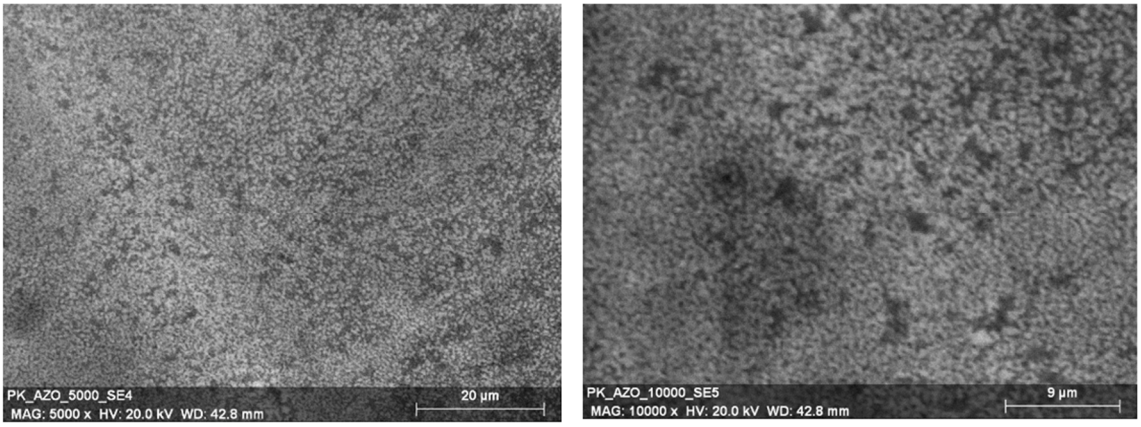


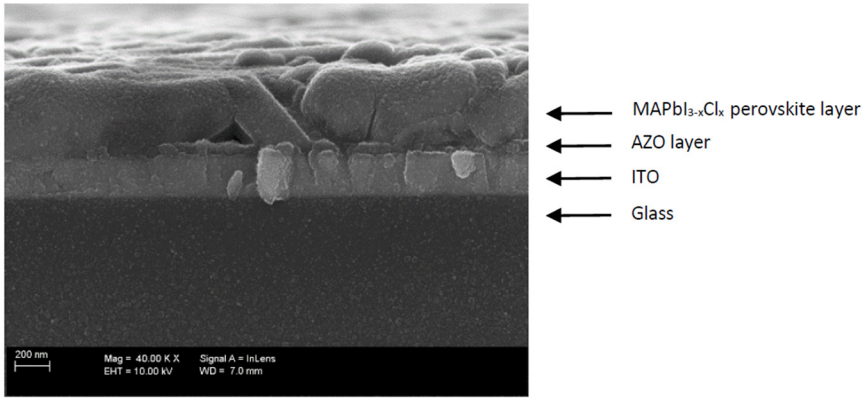
Figure S3. Photographs of the perovskite layers according to the different precursors ratio. (scale bar: 0.5 cm).



(**a**)



(**b**)



(**c**)

Figure S4. SEM images of (**a**) the AZO sub-layer (top view), (**b**) a representative $MAPbI_{3-x}Cl_x$ perovskite layer (top view), (**c**) the cross-section of an AZO based half-cell (examples for 3-1 precursors' ratio).

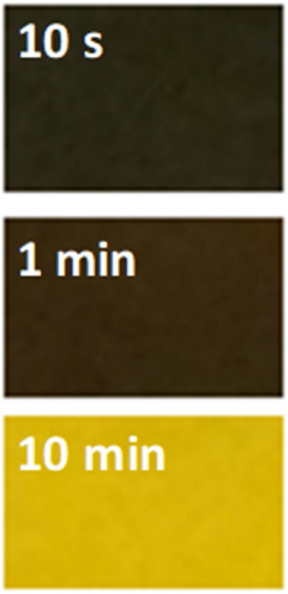


Figure S5. Photographs of a perovskite layer (example for 3-1 precursors' ratio): showing the influence of the annealing time (100 °C) on the perovskite formation and decomposition when deposited on the AZO ETL underlying layer presented in this work.

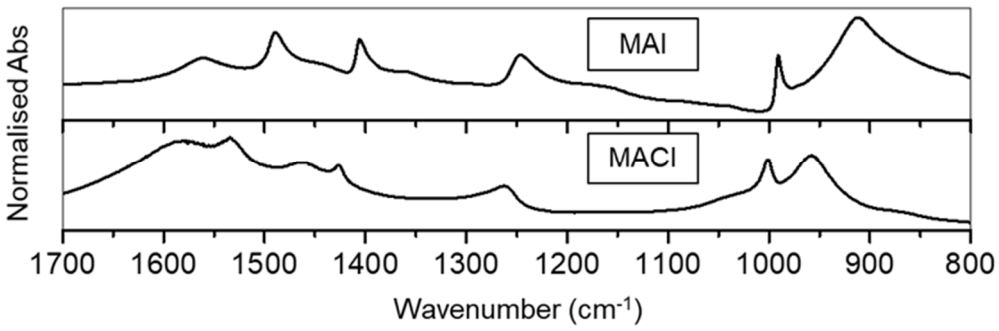


Figure 6. MACl and MAI FTIR spectra.

Table S1. Peaks assignments of IR spectra. All wavenumbers are given in cm^{-1}.

$MAPbI_3$	$MAPbCl_3$	Peak assignments
910	930	CH_3–NH_3^+ rock ν12
960	977	C–N stretch ν5
1249	1255	CH_3–NH_3^+ rock ν11
1385	Too weak	Sym. CH_3 bend ν4
1422	1431	Asym. CH_3 bend ν10
1467	1484	Sym. NH_3^+ bend ν3
1577	1594	Asym. NH_3^+ bend ν9
3127	3144	Sym NH_3^+ stretch ν1
3168	3198	Asym NH_3^+ stretch ν7